Physica C: Superconductivity and its applications 525–526 (2016) 84–88

Contents lists available at ScienceDirect

Physica C: Superconductivity and its applications

journal homepage: www.elsevier.com/locate/physc

Penetration and trapping of the magnetic flux in planar defects of $Bi_{1.65}Pb_{0.35}Sr_2Ca_{2+x}Cu_{3+x}O_y$ superconductors

M. Hernández-Wolpez[a], A. Cruz-García[b], O. Vázquez-Robaina[c], R.F. Jardim[d], P. Muné[b,*]

[a] Departamento de Física, Universidad de Camagüey, Ctra. Circunvalación Norte, Km 5 1/2, Camagüey, Cuba
[b] Departamento de Física, Universidad de Oriente, Patricio Lumumba s/n, P. O. Box 90500, Santiago de Cuba, Cuba
[c] LIEES Department, IMRE-Physics Faculty, University of Havana, Havana 10400, Cuba
[d] Instituto de Física, Universidade de São Paulo, São Paulo, 05315-970, SP, Brazil

ARTICLE INFO

Article history:
Received 28 January 2016
Revised 5 April 2016
Accepted 10 April 2016
Available online 22 April 2016

Keywords:
Bi-based superconductors
Low-angle grain boundaries
Weak links
Trapped flux

ABSTRACT

We have compared the dependence of the critical current density on maximum applied magnetic field, $J_c(0, H_{am})$, performed in pellets with the derivative of magnetization versus applied magnetic field, $dM(H_a)/dH_a$, of the corresponding powder samples of $Bi_{1.65}Pb_{0.35}Sr_2Ca_{2+x}Cu_{3+x}O_y$ samples; $x = 0.2$ and 0.5. In both cases the measurements were performed at 77 K. We have focused in the applied magnetic field range in which the magnetization as a function of applied magnetic field, $M(H_a)$, is quasi-linear. The comparison reveals that the penetration of the magnetic flux within powder particles is closely related to the trapped flux observed by means of the $J_c(0, H_{am})$ dependence in pellet samples. The combined results are well explained within the framework of the three-level superconducting model. The results also suggest that the magnetic flux, for applied magnetic fields H_a ranged from ~30 to ~80 Oe, first penetrates the intragranular planar defects, as stacking faults and/or colonies of low angle boundaries, while the magnetic flux penetration in regions free of defects is observed for higher values of H_a. As a correlative result, we have observed a decrease of the superconducting critical temperature of the crystallites T_C with increasing x, which may be related with an increase of the number of stacking faults of the material.

1. Introduction

Identifying the different and coexisting superconducting levels in samples of granular superconductors continues to be an important experimental issue of both basic and applied research on superconductivity [1]. Such an identification is closely related to a precise determination of lower critical fields H_{c1} along different orientations in these materials. As far as the latter is concerned, some authors have reported estimates of the lower critical fields in Bi-2223/Ag tapes [2]. They found that H_{c1} perpendicular to the c-axis is very low and close to 8 Oe at 77 K [2]. Similarly, estimates of H_{c1} in Bi-2223 whiskers reveal values of the lower critical field of ~60 Oe at the same temperature along the c-axis [3]. In both cases, the estimates of H_{c1} were performed following a graphic method, based on the deviation of the linear behavior of the magnetic field dependence of the magnetization data $M(H_a)$.

The mentioned values of H_{c1} may correspond to the lower intergranular critical field of a granular superconductor since those values belong to the first deviation from the linear behavior observed in the $M(H_a)$ curve obtained in polycrystalline specimens. We also mention that Job and Rosenberg [4], following a similar procedure for determining H_{c1}, have found a value of ~30 Oe in ceramic samples at 77 K. They considered this value as an estimate for the case when the magnetic field is applied parallel to the *ab* plane of the unit cell, which is a factor of 5 or 6 smaller than the case when the magnetic field is applied parallel to the c-axis, being a result consistent with the strong anisotropy of the London penetration depth in these Bi-2223 materials. However, for the reasons mentioned above, a very low value of H_{c1} may be also considered as the intergranular lower magnetic field of the granular specimen, being quite different to the one reported elsewhere [2].

Hänisch and co-authors [5] have studied the electrical transport properties of $Bi_2Sr_2Ca_2Cu_3O_{10+\delta}$ thin films with [001]-tilt grain boundaries (GBs) and different misorientation angles. They observed that an 8° GB exhibits flux creep behavior and it does not constitute a weak link. In contrast, grain boundaries with larger angles exhibit weak link behavior in this material. Similarly, Held et al. [6], measured the critical current density of the relevant $YBa_2Cu_3O_7$ GBs as a function of the misorientation angle. The authors found that, in the low angle regime, [010]-tilt boundaries and

* Corresponding author. Tel.: +53 22 630277; fax: +53 22 632689.
E-mail address: mune@uo.edu.cu (P. Muné).

http://dx.doi.org/10.1016/j.physc.2016.04.003
0921-4534/

[100]-twist boundaries reduce the critical current density much less than the observed in the [001]-tilt boundaries. In all the cases, the involved samples in the experimental work were bicrystals or thin films.

Gurevich calculated the lower critical field of a Josephson junction in the non-local limit regime [7]. His results indicate that the lower critical field is reduced in a junction as compared to one of the crystallites. Such a reduction is observed even for low misorientation angles where the flux creep regime is exhibited by the junction.

On the other hand, it is well established that the platelet-like shape of the Bi-2223 grains is responsible for the presence of different types of junctions with small angles between the *c*-axis of adjacent crystallites in the granular structure of the materials [8,9]. Depending on the type of the junction, its orientation with respect to the magnetic field, misorientation angle and demagnetization factor, the values of the so-called lower critical field H_{c1} may change appreciably when it is measured by using $M(H_a)$ data. That is probably the reason why several different values of H_{c1} are found in the literature, as above mentioned.

Powder samples of Bi-2223 have also been studied by $M(H_a)$ measurements. The obtained $M(H_a)$ curves frequently exhibit a Bean-like behavior for applied magnetic fields in the range comprehended between 0 and 500 Oe. The graphic method was also applied to determine the first critical field of the grains, which resulted to be ~80 Oe and the very high anisotropic behavior of the grains was not discussed [10,11]. Moreover, considering this value of H_{c1}, the Bi-2223 ceramic samples were interpreted as being constituted by three superconducting levels, or more appropriately, by superconducting grains, superconducting clusters (strong links among grains), and weak links [10,11]. To confirm the presence of the others two superconducting levels besides the superconducting grains, the dependence of the critical current density as a function of the "historic" applied magnetic field, $J_c(0, H_{am})$, and the critical current density in increasing applied magnetic fields $J_c(H_a)$ were also considered.

The intrinsic anisotropy of superconductors causes a dependence of the intragranular lower critical fields with respect to the angle between the magnetic field and the main axis of the crystallites (*c*-axis), following the expression written below (see, for example, Ref. [12])

$$H_{c1}(\gamma) = H_{c1}^{c}\left(\cos^2(\gamma) + \frac{m_c}{m_{ab}}\sin^2(\gamma)\right)^{1/2}. \quad (1)$$

Here, γ, m_c, and m_{ab} are the angle between the *c*-axis and the magnetic field, and the anisotropic components of the mass tensor, respectively. As a consequence, in a powder sample or pellet with random orientation of the grains, a wide distribution of lower critical field values may be observed due to the high anisotropy of the system. However, the $M(H_a)$ curves of powder samples were observed to follow the Bean model [13] with a lower critical field H_{c1} ~80 Oe, as mentioned previously [10,11].

Within this challenging context, we have compared the results extracted from the $M(H_a)$ dependence of powder samples with those related to the so-called flux-trapping curve, $J_c(0, H_{am})$ [14], measured in pellet samples of the same material. A close relationship between both processes, i.e., penetration of the magnetic flux and trapping of the magnetic flux, has been observed even when they occur independently in powder and pellet samples, respectively. As complementary characterization of the samples, we discuss the results of X-ray diffraction, scanning electron microscopy (SEM), and magnetization as a function of temperature $M(T)$. Our experimental results reveal that the superconducting clusters may be viewed as defects inside grains instead of grains with strong links between them, as described elsewhere [10,11]. Moreover, the trapped flux seen in $J_c(0, H_{am})$ data within the magnetic field interval $30 < H_{am} < 80$ Oe of maximum applied magnetic field is related to these defects inside the crystallites (grains) [4,15–17] which are believed to act as large Josephson junctions. Thus, the critical field to create a vortex in those regions is less than that belonging to crystallites without defects [7]. Finally, our results offer a method to create, detect, and study intragranular defects in Bi-2223 polycrystalline superconductors, a procedure that could be extended to other layered high T_C superconductors.

2. Experimental

Samples of Bi-2223 were elaborated following the preparation route described elsewhere [10]. The starting compositions were $Bi_{1.65}Pb_{0.35}Sr_2Ca_{2+x}Cu_{3+x}O_y$ with $x = 0.2$ (D1) and 0.5 (D2) and the final compacting pressure 298 MPa. From the same pellet, two types of samples were extracted: powder and slabs for measurements of $M(H_a)$ and flux-trapping curves, respectively. A piece of the pellets was manually milled during close to 15 min to obtain the powder samples.

The phase purity of the samples was investigated by XRD using CuKα radiation and also were calculated the unit-cell dimensions of both samples (D1 and D2). Powder diffraction patterns were collected at room temperature with a Brucker D8 Advanced diffractometer by using the scanning mode with a step size $\Delta(2\Theta) = 0.05^\circ$ and $3^\circ < 2\Theta < 80^\circ$ during 3 s of counting time.

The average grain size of both powder and pellet samples was determined by using scanning electron microscopy (SEM). The micrographies were taken with the help of a Scanning Electron Microscope Hitachi S-530. The platelet like shape of the grains, a fingerprint feature of Bi-2223 samples, was also observed.

Magnetization versus temperature in powder samples, $M(T)$ were measured by using a commercial Quantum Design SQUID magnetometer. In these measurements the powders were cooled in zero applied magnetic field from room temperature down to 5 K. Then, a magnetic field of 5 Oe was applied, the temperature was increased in steps of 2 K, and the magnetization data $M(T)$ were collected up to 120 K.

Magnetization measurements under low applied magnetic fields were performed by using a commercial Quantum Design SQUID magnetometer. In this experiment the powder samples were cooled in zero applied magnetic field from room temperature down to 77 K. After that, the applied magnetic field, H_a, was then increased from 0 to 500 Oe, in steps of 5 Oe and the magnetization was measured for each value of H_a.

On the other hand, measurements of the critical current density as a function of applied "historic" magnetic field, $J_c(0, H_{am})$, were performed using the standard dc four-probe technique in a slabs with typical dimensions of $d = 0.5$ mm (thickness), $w = 2$ mm (width) and $l = 10$ mm (length). The samples were cooled in the same conditions as described above. Then, a certain value of maximum magnetic field, H_{am}, was applied to the samples for approximately 30 s, after which it was reduced to zero again, and the critical current density was determined by using the criterion of 1 μV. Finally, the samples was warmed up to temperatures higher than the superconducting critical temperature in order to erase its magnetic "memory" and then cooled down again to 77 K in zero applied magnetic fields. By repeating these steps for different values of B_{am}, the flux-trapping curves, $J_c(0, H_{am})$, were built [14].

3. Results and discussion

From the X-ray powder diffractograms, displayed in Fig. 1, we have found that both samples have similar peak profiles. The two samples D1 and D2 are comprised of a mixture of phases in which the Bi-2223 phase coexists with two extra phases such as Bi-2212 and Ca_2PbO_4. We have estimated that the materials are

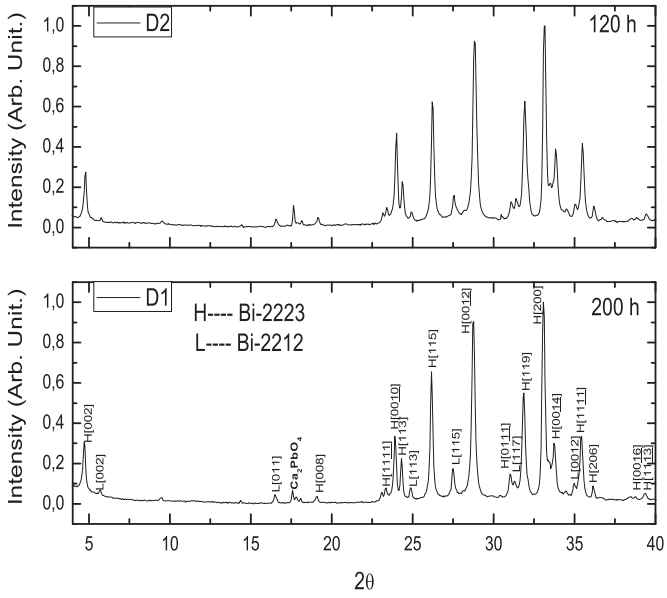

Fig. 1. X-ray diffraction patterns for the powder samples D1 and D2, respectively.

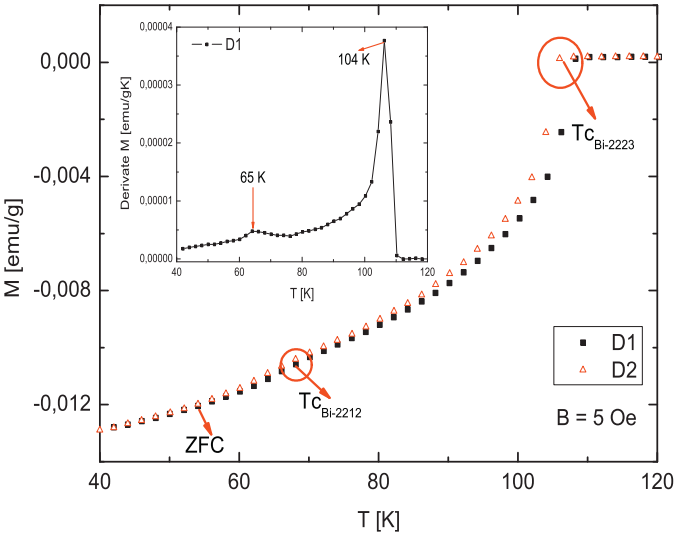

Fig. 2. Magnetization as a function of temperature in the powder samples D1 and D2. The inset shows dM/dT as a function of temperature for the powder sample D1.

comprised of ~83% of the Bi-2223 phase and ~17% of the extra phases. The unit-cell parameters were calculated with respect to an orthorhombic unit cell (Bi-2223 phase) and the obtained values for sample D1 were: $a = 5.412$ Å, $b = 5.345$ Å, and $c = 37.212$ Å, while the values for sample D2 were: $a = 5.402$ Å, $b = 5.423$ Å, and $c = 37.152$ Å. These calculated values are in agreement with the one reported elsewhere [11] when the experimental uncertainties are considered. In addition to this, the most important difference between the obtaining process of both samples is related to the sintering time. It seems to be that with increasing the dopant quantities, decrease the sintering time to obtain certain percent of the high critical temperature phase (Bi-2223). At the same time, increasing dopant quantities favor the trapping flux process at low maximum applied magnetic fields $H_{am} < 80$ Oe as described below. To identify the cause of this behavior an additional technique was used to study the influence of the extra phases.

Measurements of magnetization as a function of temperature, shown in Fig. 2, were performed to both powder samples in order to clarify the influence of the extra phases in the superconducting

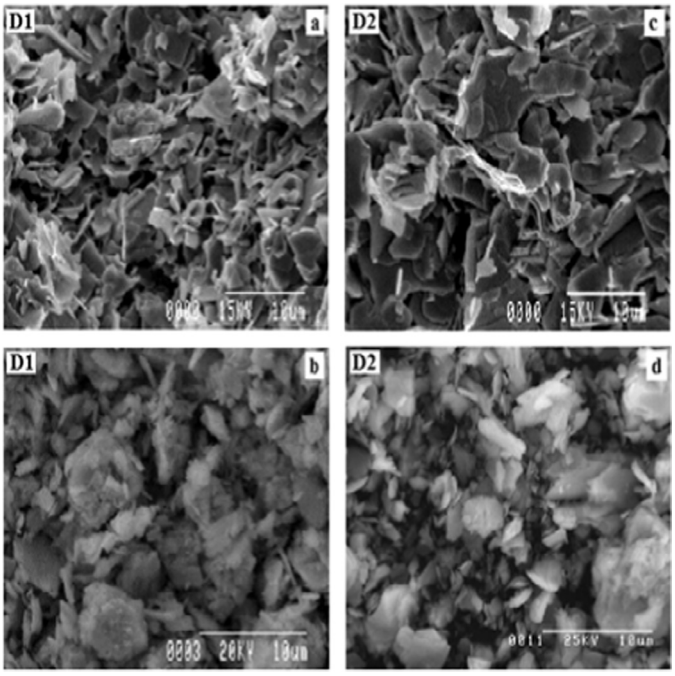

Fig. 3. Micrographs of the samples D1 (a, b) and D2 (c, d).

properties of these samples. A careful inspection of these curves allows us to confirm that the extra phase Bi-2212 does not participate as superconducting phase in the overall behavior of the samples because their critical temperature is ~65 K (see insert of Fig. 2) and the experimental data related to the penetration and trapping of the magnetic flux were collected at 77 K. We show, as an example, the derivative of $M(T)$ for the D1 sample. A small, but clear maximum is observed at 65 K. The result for the D2 sample is similar. Another important feature to be analyzed from the data displayed in Fig. 2 is the decrease of the superconducting critical temperature at which the superconducting transition of the Bi-2223 phase starts when the doping is increased. However, the $M(T)$ curves are very similar for $T < 80$ K.

Fig. 3 shows two SEM images corresponding to samples D1 and D2. Two of them belong to the fractured surfaces pellet samples (a, c) and the others to the powder samples (b, d). It is possible to observe that the granular morphology of both samples is similar, exhibiting clearly the occurrence of grains with platelet-like shape mainly in pellet samples (a, c) of both specimens. The differences of the dopant concentrations do not provoke appreciable changes in the granular morphology of the ceramics judging by the mean grain size which is the same for both specimens: $L_a \sim 6$ μm and $L_c \sim 0.6$ μm for the pellet samples and $L_a \sim 5$ μm and $L_c \sim 0.5$ μm for the powder samples. Here the subscripts a and c represent the dimensions of the crystallites for the ab plane and the c direction, respectively. These results are in perfect agreement with those reported elsewhere [10].

In Fig. 4 the $M(H_a)$ curves for both samples are shown. These curves exhibit a quasi-linear behavior in the interval $0 < H_a < 80$ Oe apparently related to the Meissner state of the grains of the powder samples. The curves display also a Bean-like behavior [13] in the whole range of applied magnetic field $0 < H_a < 500$ Oe. In order to analyze in details the flux penetration process within the grains we have also plotted the $dM(H_a)/dH_a$ curves in Fig. 5(a). Notice that for $30 < H_a < 80$ Oe the dependence shows several steps, but its increase is more continuous and regular for $H_a > 80$ Oe in both cases. Similar behavior is also observed in the flux-trapping curves which are displayed in Fig. 6. These

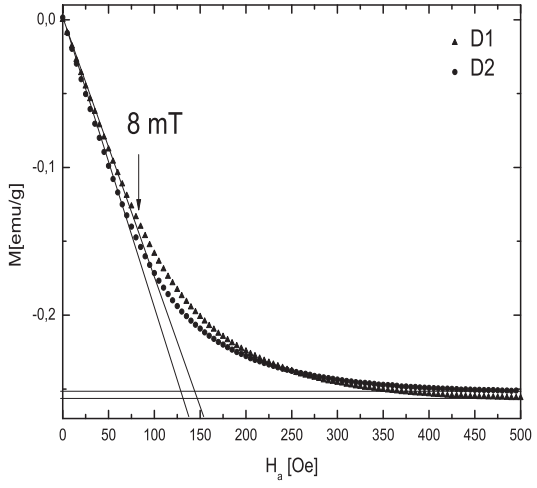

Fig. 4. Magnetization as a function of the applied magnetic field of the powder samples D1 and D2. The continuous lines evidence the quasi-linear and saturation regions.

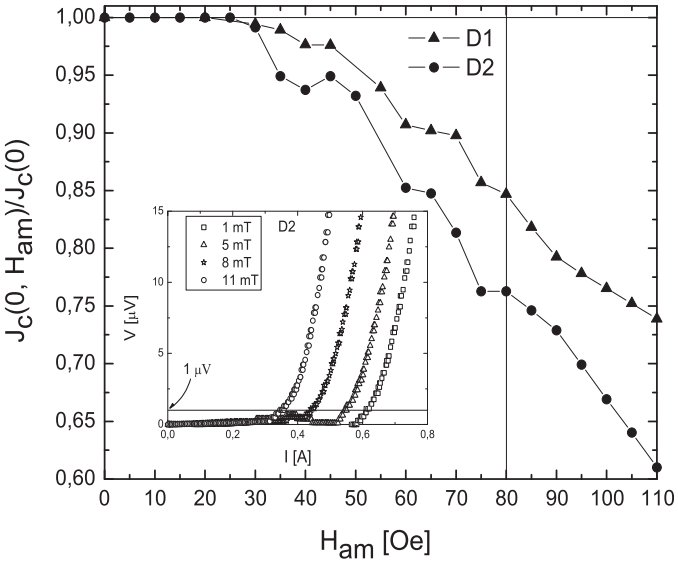

Fig. 6. Flux-trapping curves of the pellet samples D1 and D2. The continuous horizontal and vertical lines marked the values of $J_c(0, H_{am})$ at $H_{am} = 0$ and the value of the applied magnetic field of 80 Oe, respectively. The inset shows some I–V curves measured on the sample D2 starting from which the flux-trapping curve is built.

results suggest that the penetration of the magnetic flux and the flux trapping processes in powder and pellet samples, respectively, are closely related. If this were the case, the main cause of the $J_c(0, H_{am})$ behavior may be related to the intragranular trapped flux,

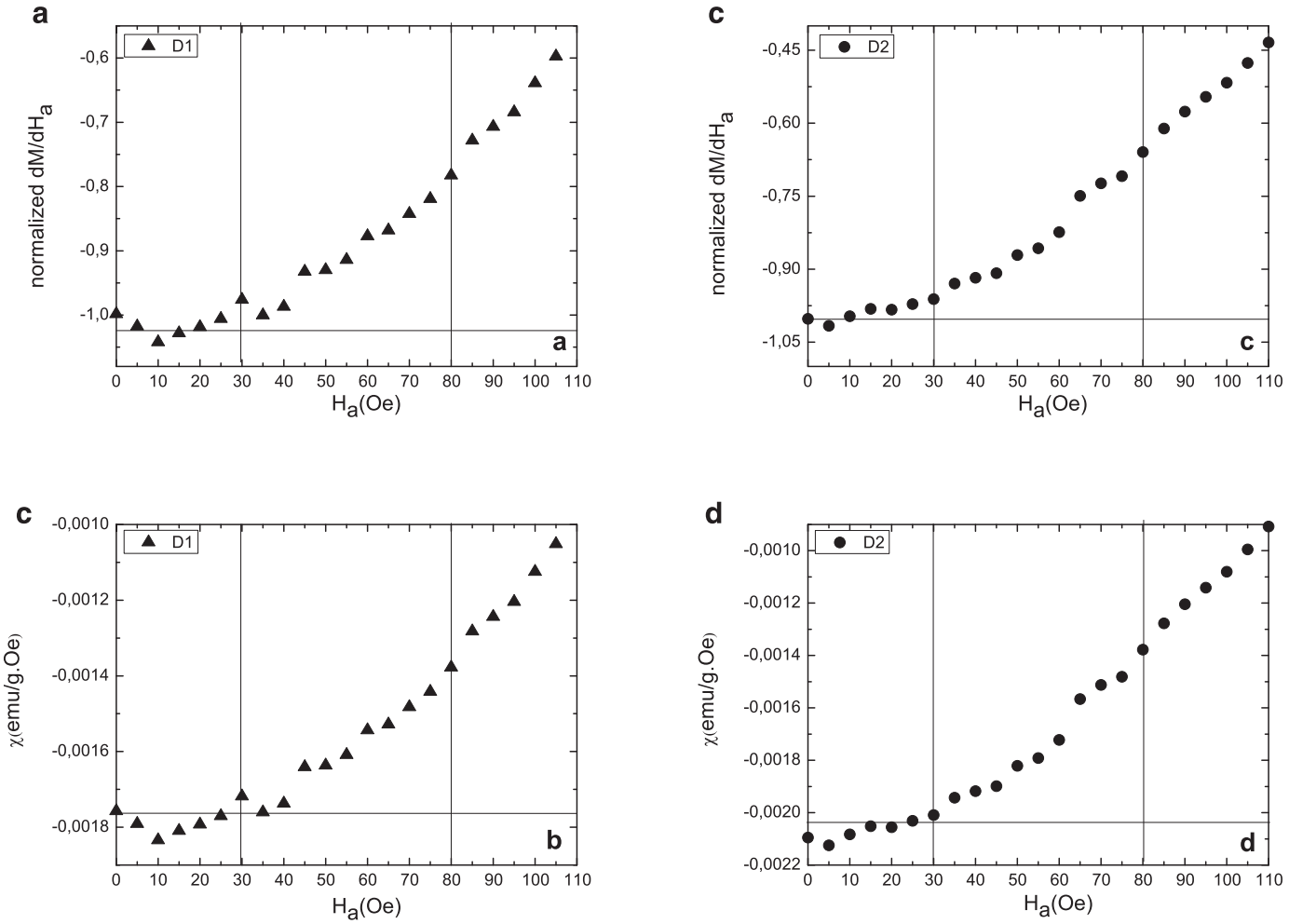

Fig. 5. (a) and (c) Normalized $dM(H_a)/dH_a$ as a function of applied magnetic field of the powder samples D1 and D2, respectively. (b) and (d) Dependences of the ratio M/H_a versus H_a of the powder samples D1 and D2, respectively. The continuous horizontal and vertical lines visualize the value of dM/dH_a at $H_a = 0$ and $30 < H_a < 80$ Oe interval, respectively.

contrary to the concept of superconducting cluster described elsewhere [10,11]. Another important feature to be considered here is that the D2 sample exhibits a more pronounced flux trapping and penetration effects observed by means of the curves $dM(H_a)/dH_a$ and $J_c(0, H_{am})$, respectively. To summarize the experimental results described up to now we have considered the following issues:

1. For $H_a < 30$ Oe the effect of the magnetic flux penetration or trapping, as seen in curves of Figs. 5(a) and (c), are negligible and are disregarded.
2. For $30 < H_a < 80$ Oe two processes are believed to occur: (i) the superconducting grains are penetrated in defects; (ii) due to the effect of flux compression, the magnetic flux penetrates first in superconducting grains with high demagnetization factors. It is important to point out that the lower critical fields of the defects are, as a general rule, lower than those belonging to other regions of the superconducting crystallites free of defects. Thus, in the presence of planar defects, the magnetic flux penetrates first at the defects and then at the regions of the crystallites free of defects for higher values of applied magnetic field. Another issue to be considered is the existence of several jumps in this region (see Fig. 5(a) and (c)). It could be due to the derivative process employed, but plotting the dependence of the ratio M/H_a versus H_a (see Fig. 5(b) and (d)), the obtained results are similar. Hence, it can to set out that this feature depends on the intrinsic behavior of the samples. Moreover, different dopings vary the effects of the penetration and trapping of the magnetic flux in powder and pellet samples, however it does not affect appreciably the granular morphology of the samples. Thus, the effects of the demagnetization factors of the grains are not decisive in the behavior of the samples.
3. For $H_a > 80$ Oe most of the grains start to be penetrated by the magnetic flux in the regions free of defects.

The discontinued growth of the $dM(H_a)/dH_a$ curves in the second magnetic field interval can be explained by assuming the penetration of the magnetic flux into defects of the grains. For certain values of the applied magnetic field these defects are penetrated depending on their specific features such as misorientation angle [16,18] intrinsic characteristics, and also the defects orientation with respect to the intergranular magnetic field [19]. Such a penetration provokes jumps in the $dM(H_a)/dH_a$ dependence. It happens because in the defects the magnetic flux penetration is confined to the junction area of order $2\lambda L$. Here, L represents the length of the defect between two crystallites and λ is the London penetration depth [20]. On the other hand, when the magnetic flux penetrates into the regions free of planar defects of the superconducting grains, the $M(H_a)$ curves follow the Bean model [13] and the increase of its slope is continuous, as observed in the third interval of the applied magnetic field in the curves displayed in Fig. 5. Due to the high intrinsic anisotropy of the Bi-2223 grains, we consider that the first penetrations of the magnetic flux into the defects and crystallites properly must happen in those crystallites oriented with their c-axis perpendicular to the intergranular magnetic field [4]. Nevertheless, considering the high shape anisotropy of the grains, the penetration in planar defects parallel to the c-axis of the crystallites may also happen. It agrees with the presence of brick-wall structure of twist boundaries inside the grains [16], the value of $H_{c1}= 60$ Oe obtained in whiskers for magnetic field applied along the c-axis [3], and the experimental fact that the $M(H_a)$ curves does not reflect the high intrinsic anisotropy of the crystallites. A superposition of the penetration processes along both perpendicular directions of the crystallites may explain this latter experimental feature (see Fig. 4). Finally, we are offering here a procedure for creating, detecting and studying intragranular defects in Bi-2223 powders and low compacted samples, which can be extended to other high T_C superconductors. Another paper with a quantitative model is in progress.

4. Conclusions

In summary, we have observed a well defined correlation between the magnetic flux penetration in powder specimens of Bi-2223 and the transport flux-trapping curves measured in slabs of the same material. The results indicate that the magnetic flux trapping in ceramic samples, subjected to low uniaxial compacting pressures, may be considered an intragranular phenomenon. Moreover, the penetration and trapping flux of Bi-2223 ceramic samples at the applied magnetic field interval of $30 < H_a < 80$ Oe has been observed in several different types of ceramic samples. According to our results this experimental feature is closely related to the existence of intragranular defects as colonies of low-angle c-axis boundaries, brick-wall structure of twist boundaries and *stacking faults* or absence of Cu-O planes [7,15–18]. These defects manifest themselves in our magnetic data as a distribution of lower critical fields less than the value that corresponds to crystallites free of defects. Considering the high intrinsic anisotropy of the Bi-2223 superconductors, the magnetic flux penetrates first the defects of the crystallites oriented with their c-axes perpendicular to the intergranular magnetic field and then the crystalline regions free of planar defects. However, due to the high shape anisotropy of the Bi-2223 crystallites, a superposition of the penetration processes in both perpendicular direction of them cannot be disregarded. Finally, the doping with Cu and Ca of the samples may increase the defects, making weaker the connection between the Cu-O planes along to the c-axis. Under these circumstances, the doping decreases the superconducting energy gap of the Bi-2223 phase and thus decreasing its superconducting critical temperature.

Acknowledgment

This work was supported by Brazil's agencies FAPESP (Grant nos. 2013/07296-2 and 2014/19245-6), CNPq, and CAPES under CAPES/MES Grant no. 104/10.

References

[1] L. Ji, M.S. Rzchowski, N. Anand, M. Tinkham, Phys. Rev. B 47 (1993) 470.
[2] M. Majoros, L. Martini, S. Zainella, Physica C 282 (1997) 2205.
[3] I. Matsubara, R. Funahashi, K. Ueno, H. Yamashita, T. Kawai, Physica C 256 (1996) 33.
[4] R. Job, M. Rosenberg, Physica C 172 (1991) 391.
[5] J. Hänisch, A. Attenberger, B. Holzapfel, L. Shultz, Phys. Rev. B 65 (2002) 052507.
[6] R. Held, C.W. Schneider, J. Mannhart, L.F. Allard, K.L. More, A. Goyal, Phys. Rev. B 79 (2009) 014515.
[7] A. Gurevich, Phys. Rev. B 46 (1992) R3187.
[8] A.P. Malozemoff, in: S.H. Whang, A. DasGupta, R.B. Laibowitz (Eds.), High Transition Temperature Compounds II, TMS, Warrendale, PA, 1990, p. 3.
[9] A. Umezawa, Y. Feng, H.S. Edelman, Y.E. High, D.C. Larbalestier, Y.S. Sung, E.E. Hellstrom, Physica C 261 (1992) 198.
[10] P. Muné, Govea-Alcaide, R.F. Jardim, Physica C 384 (2003) 491.
[11] E. Govea-Alcaide, R.F. Jardim, P. Muné, Physica C 423 (2005) 152.
[12] V.A. Finkel, Low Temp. Phys. 25 (1999) 410.
[13] C.P. Bean, Rev. Mod. Phys. 36 (1964) 31.
[14] E. Altshuler, S. García, J. Barroso, Physica C 177 (1991) 61.
[15] V. Kataev, N. Knauf, B. Buchner, D. Wohlleben, Physica C 184 (1991) 165.
[16] A. Gurevich, L.D. Cooley, Phys. Rev. B 50 (1994) 13563.
[17] K. Kishida, N.D. Browning, Physica C 351 (2001) 281.
[18] M. Mora, in: Tesis de doctorado, Universidad de Zaragoza, España, 1998.
[19] P. Muné, M.H. Wolpez, A.C. García, R.F. Jardim, Rev. Cub. Fis. 32 (2015) 53.
[20] A. Gurevich, M.S. Rzchowski, G. Daniels, S. Patnaik, B.M. Hinaus, F. Carillo, F. Tafuri, D.C. Larbalestier, Phys. Rev. Lett. 88 (2002) 097001.